

Elastic properties and electronic structures of antiperovskite-type InNCo_3 and InNNi_3

Z. F. Hou

Department of Physics, Fudan University, Shanghai, 200433, P. R. China

Abstract

We have performed the first-principles calculations to study the elasticity, electronic structure, and magnetism of InNCo_3 and InNNi_3 . The independent elastic constants are derived from the second derivative of total energy as a function of strain, and the elastic modulus are predicted according to the Voigt-Reuss-Hill approximation. Our calculations show that the bulk modulus of InNCo_3 is slightly larger than that of InNNi_3 due to a smaller lattice constant for InNCo_3 . For InNCo_3 the ferromagnetic state is energetically preferable to the paramagnetic state, while the ground state of InNNi_3 is a stable paramagnetic (non-magnetic) state. This is due to the different strength of $2p$ - $3d$ hybridization for the N-Co and N-Ni atoms in InNCo_3 and InNNi_3 .

I. INTRODUCTION

The ternary nitrides or carbides with the general formula AXM_3 (A: divalent or trivalent element; X: carbon or nitrogen; and M: transition metal) are already known for several decades¹⁻³. These compounds crystalize in a cubic anti-perovskite structure (A: cube-corner position; X: body-center position; M: face-center position) and exhibit a wide range of interesting physical properties¹, such as giant magneto-resistance⁴ and nearly zero temperature coefficient resistivity⁵. They have renewedly attracted considerable attention due to the discovery of superconductivity at ~ 8 K in intermetallic compound $MgCNi_3$ ⁶.

Considering the Ni-rich composition, it is expected that the ferromagnetism could exist in $MgCNi_3$. However, the absence of ferromagnetism was observed in experiment⁶ for $MgCNi_3$. From the electronic structures obtained by the first-principles calculations⁷⁻¹⁰, the non-ferromagnetic ground state of $MgCNi_3$ is ascribed to a reduced Stoner factor that results from a strong hybridization between the Ni-3d and C-2p electrons. For other Ni-based ternary carbides $ACNi_3$ (e.g., A = Al, Ca, In, Zn, and Cd), the first-principles calculations¹⁰⁻¹⁴ also show that the ground states of these compounds are non-magnetic and the C-Ni bonding exhibits nearly same characteristics as the one in $MgCNi_3$. Therefore, this indicates that the change of composition A could not induce the ferromagnetism in $ACNi_3$. On the other side, it raises a question whether the change of composition X or M can lead to the appearance of ferromagnetism in AXM_3 or not.

Very recently, the antiperovskite-type compounds InN_yCo_3 and InN_yNi_3 ($y \sim 1.0$ and 0.8 , respectively) have been synthesized by solid-gas reactions of metal powders with NH_3 and they have been reported to have spin-glass-like properties based on the measurements of temperature dependence magnetization.¹⁵ The recent first-principles calculations¹² showed that the non-stoichiometry could affect the magnetic properties of $ACNi_3$ (e.g., $AlCNi_3$ and $GaCNi_3$) and suggested that the tendencies toward magnetism found in experiments¹⁶⁻¹⁹ for these compounds should be explained by the deviation of the Ni/C atomic ratio from the ideal stoichiometry. To shed more light on the understanding on the magnetic properties of $InNCo_3$ and $InNNi_3$ reported in experiment¹⁵, it is of great importance to theoretically study the electronic structures of these two compounds as well as the nature of the N-Co and N-Ni bondings.

In order to completely understand the electronic structures and magnetic ground states of

InNiCo₃ and InNiNi₃ with cubic anti-perovskite structure, we carried out the first-principles calculations on these compounds using the pseudopotentials method with plane-wave basis set within the local density approximation and the generalized gradient approximation. Since the elastic properties of a solid are highly associated with various fundamental solid-state properties such as phonon spectra, specific heat, Debye temperature, and so on, we have calculated the independent elastic constant and the elastic moduli of InNiCo₃ and InNiNi₃.

II. COMPUTATIONAL DETAILS

All calculations on antiperovskite-type InNiCo₃ and InNiNi₃ were performed using the Quantum ESPRESSO code²⁰, which is based on the density functional theory (DFT)²¹. The electronic exchange-correlation potential was calculated within the local density approximation (LDA)^{22,23} and the generalized gradient approximation using the scheme of Perdew-Burke-Ernzerhof (PBE)²⁴. The spin polarization was also considered in the calculation in order to assess the magnetic properties of these compounds. Electron-ion interaction was represented by the norm-conserving optimized²⁵ designed nonlocal pseudopotentials. The 4*d* electrons are explicitly included in the valence of In. The electronic wavefunctions were expanded by the plane waves up to a kinetic energy cutoff of 55 Ry. The **k**-point sampling in Brillouin zone (BZ) of simple cubic lattice was treated with the Monkhorst-Pack scheme²⁶ and a 20×20×20 **k**-point mesh (i.e., 286 irreducible points in the first BZ) was used. The chosen plane-wave cutoff and number of **k** points were carefully checked to ensure that the total energy was converged to be better than 1 mRy/cell. The total energies are obtained as a function of volume and they are fitted with the Birch-Murnaghan 3rd-order equation of states (EoS)²⁷ to give the equilibrium lattice constant and other ground state properties. During the calculation of density of states (DOS), a dense **k**-point mesh of 30×30×30 is used, the total DOS is computed by the tetrahedron method²⁸, and the atomic-projected DOS is calculated by the Löwdin populations²⁹.

For a cubic crystal, its independent elastic constants are c_{11} , c_{12} , and c_{44} . To determine the elastic constants of InNiCo₃ and InNiNi₃ by means of the curvature of the internal energy versus the strain curves^{30,31}, three strain modes³² are adopted and their nonzero strains are as follows: (1) $\epsilon_{11} = \epsilon_{22} = \delta$, $\epsilon_{33} = (1 + \delta)^{-2} - 1$; (2) $\epsilon_{11} = \epsilon_{22} = \epsilon_{33} = \delta$; and (3) $\epsilon_{12} = \epsilon_{21} = \delta/2$, $\epsilon_{33} = \delta^2/(4 - \delta^2)$. The deformation magnitudes δ from -0.012 to 0.012

in the step of 0.03 are applied in the first and second strain modes, and δ from -0.04 to 0.04 in the step 0.01 are adopted in the third strain mode. Once the independent elastic constants for single crystal properties are obtained through the above procedure, the elastic moduli (e.g., the shear modulus and the bulk modulus) of polycrystalline aggregates can be estimated according to the Voigt-Reuss-Hill approximation³³⁻³⁵. In the Voigt average³³, the shear modulus and the bulk modulus of cubic lattice are given by

$$G_V = \frac{1}{5} [(c_{11} - c_{12}) + 3c_{44}] \quad (1)$$

and

$$B_V = \frac{1}{3}(c_{11} + 2c_{12}), \quad (2)$$

while in the Reuss average³⁴ they are given by

$$G_R = \frac{5}{4(s_{11} - s_{12}) + 3s_{44}} \quad (3)$$

and

$$B_R = \frac{1}{3s_{11} + 6s_{12}} \quad (4)$$

with the relations $c_{44} = s_{44}^{-1}$, $c_{11} - c_{12} = (s_{11} - s_{12})^{-1}$, and $c_{11} + 2c_{12} = (s_{11} + 2s_{12})^{-1}$ in the cubic lattice, where s_{ij} are the elastic compliance constants. Therefore, G_R and B_R in the cubic lattice can be rewritten as

$$G_R = \left[\frac{4}{5}(c_{11} - c_{12})^{-1} + \frac{3}{5}c_{44}^{-1} \right]^{-1}, \quad (5)$$

and

$$\begin{aligned} B_R &= \frac{1}{3} [(c_{11} + 2c_{12})] \\ &= B_V. \end{aligned} \quad (6)$$

In the Hill empirical average³⁵, the shear modulus and the bulk modulus are taken as $G = \frac{1}{2}(G_V + G_R)$ and $B = \frac{1}{2}(B_V + B_R)$, respectively. Knowing G and B , the Young's modulus E and Poisson's ratio ν , which are frequently measured for polycrystalline materials when investigating their hardness, can be calculated from the isotropic relations:

$$E = \frac{9BG}{3B + G} \quad (7)$$

and

$$\nu = \frac{3B - 2G}{2(3B + G)}. \quad (8)$$

III. RESULTS AND DISCUSSIONS

A. Structural properties

In experiment with the powder X-ray diffraction patterns, Cao et al¹⁵ have reported that InN_yCo_3 and InN_yNi_3 ($y \sim 1.0$ and 0.8 , respectively) have the cubic anti-perovskite structure with the space group $221(Pm\bar{3}m)$ and the corresponding lattice parameters were 3.854 \AA and 3.844 \AA , respectively. Starting from the experimental data, we have calculated the total energies of unit cell at a series of volumes for each compound in the paramagnetic (PM) and ferromagnetic (FM) states. The results are presented in Fig. 1. It is found that the energy difference between the FM and PM states is -0.0397 eV (-0.226 eV) in the LDA (GGA) calculations for InNCo_3 and 0.0 eV for InNNi_3 . The total magnetic moment of InNCo_3 is about $2.14 \mu_B$ ($2.91 \mu_B$) and the local magnetic moment of each In ion is about $0.69 \mu_B$ ($0.94 \mu_B$) in LDA (GGA) calculations. The total magnetic moment of InNNi_3 and the local magnetic moment of each Ni atom are zero. These indicate that the ferromagnetic state is energetically favorable to InNCo_3 and the ground state of InNNi_3 is paramagnetic state (non-magnetic). The obtained equilibrium lattice constant (a_0), bulk modulus (B), and first pressure derivative of bulk modulus (B') of InNCo_3 and InNNi_3 are listed in Table I. In our calculations, the predicted lattice constant of InNCo_3 is slightly larger than that of InNNi_3 , which is opposite to the trend reported in experiment¹⁵. This may be due to the deviation of the Ni/N atomic ratio from the ideal stoichiometry in experiment for InN_yNi_3 . In addition, it can be seen that the deviations of the LDA (GGA) lattice constants of both the InNCo_3 and InNNi_3 with respect to the experimental values are less than 2.6% (1.0%). That is to say, the calculated equilibrium lattice constants of InNCo_3 and InNNi_3 are in excellent agreement with the experimental data¹⁵.

B. Elastic properties

The calculated independent elastic constants for single crystal of InNCo_3 and InNNi_3 are listed in Table II. Based on the Voigt-Reuss-Hill approximation^{33–35}, the elastic moduli of InNCo_3 and InNNi_3 are estimated and the results are listed in Table II. For the bulk moduli of InNCo_3 and InNNi_3 , the estimations based on the independent elastic constants agree well those obtained by the fit of the Birch-Murnaghan 3rd-order EoS. To the best of

our knowledge, no experimental data or theoretical results for the elasticity of InNCo_3 and InNNi_3 compounds have been reported up to now. Considering that the elastic properties of ZnNNi_3 , InNSc_3 , and InCNi_3 with cubic anti-perovskite structure have been studied recently and the theoretical results are available in literature^{14,36–38}, it will be meaningful to compare them with those of InNCo_3 and InNNi_3 compounds. The order of bulk moduli of these five compounds from low to high is: $B(\text{InNSc}_3) < B(\text{InNNi}_3) < B(\text{InCNi}_3) < B(\text{InNCo}_3) < B(\text{ZnNNi}_3)$. This could be understood from the trend in lattice constants (a) of these compounds (i.e., $a(\text{InNSc}_3) > a(\text{InNNi}_3) > a(\text{InCNi}_3) > a(\text{InNCo}_3) > a(\text{ZnNNi}_3)$) as well as the relationship between bulk modulus and equilibrium volume (i.e., $B \sim V^{-1}$)³⁹. The GGA lattice constants of InNSc_3 , ZnNNi_3 , and InCNi_3 are 4.411 Å³⁶, 3.77 Å³⁷, and 3.880 Å¹⁴, respectively. The order of shear modulus from low to high is: $G(\text{ZnNNi}_3 \text{ and } \text{InNNi}_3) < G(\text{InCNi}_3) < G(\text{InNCo}_3)$. Pugh⁴⁰ has proposed that a high B/G ratio may be associated with better ductility whereas a low value would correspond to a more brittleness, and the critical value separating ductile and brittle materials is around 1.75. From the results of B/G ratio for InNCo_3 , InNNi_3 , InNSc_3 , ZnNNi_3 , and InCNi_3 , it is found that only InNSc_3 can be classified as brittle materials and others may be ductile materials. Furthermore, InNNi_3 seems to be more ductile than InNCo_3 .

For a cubic crystal, its mechanical stability requires that its three independent elastic constants should satisfy the following relations⁴¹:

$$(c_{11} - c_{12}) > 0, c_{11} > 0, c_{44} > 0, (c_{11} + 2c_{12}) > 0. \quad (9)$$

These conditions also lead to a restriction on the magnitude of B :

$$c_{12} < B < c_{11}. \quad (10)$$

The predicted c_{ij} values (see Table II) for InNCo_3 and InNNi_3 satisfy these conditions, indicating that cubic antiperovskite-type compounds InNCo_3 and InNNi_3 are mechanically stable.

C. Electronic structures

In order to understand the different magnetic ground states for InNCo_3 and InNNi_3 , we examined the electronic structures of these two compounds. For the simplicity in discussion,

only the GGA results are presented below. The calculated electronic band structures along the high symmetry directions in the Brillouin zone are shown in Fig. 2. As discussed above, for InNCo_3 the ferromagnetic state is energetically preferable to the paramagnetic state, and hence it is clearly seen that the spin-splitting occurs in the bands around the E_F . For InNCo_3 the profile of majority spin bands looks roughly similar to the one of minority spin bands, however only one band in the majority spin bands crosses the Fermi level and the corresponding band with same dispersion in the minority spin bands is unoccupied. In addition, two bands in the minority spin bands across the Fermi level of InNCo_3 (see Fig. 2(a)). For InNNi_3 the ferromagnetic state is not energetically preferable to the paramagnetic state, consequently, the majority and minority spin bands are degenerated, that is to say, no spin-splitting occurs in the band structure (see Fig. 2(b)). It is interesting to note that the whole feature of majority spin bands of InNNi_3 is very similar to the one of InNCo_3 . In order to reveal the detailed character of band structure, the total density of states (DOS) and the angular-momentum-projected DOS of each atom in InNCo_3 and InNNi_3 are presented in Fig. 3. For both InNCo_3 and InNNi_3 , the four bands from -9 eV to -5 eV come mainly from the N $2p$ states and In $5s$ states, and the five bands roughly from -5 eV to -2.5 eV have significant contribution from $3d-t_{2g}$ states of transition metal atoms (Co/Ni) and the $5p$ state of In atom. For the bands from -2.5 eV to 0 eV (i.e., the Fermi level), they are dominated by the $3d$ states of transition metal atoms (Co/Ni) and have small contribution from the $2p$ states of N atom. Because the number of $3d$ electrons in Co is one less than that of Ni, two minority spin bands composed of the $3d-t_{2g}$ states around the Fermi level are unoccupied in InNCo_3 , while the counterpart in the InNNi_3 are occupied. This also results in different behavior of spin-splitting in InNCo_3 and InNNi_3 . Due to the significant spin-splitting around the Fermi level in InNCo_3 , the hybridization between the Co $3d$ and N $2p$ states in InNCo_3 are slightly weaker than the one between Ni $3d$ and N $2p$ states in InNNi_3 (see Fig. 3).

The contributions of each kind of atoms to the DOS at the E_F of InNCo_3 and InNNi_3 are listed in Table III. The total DOS at the E_F of InNCo_3 is about 2.761 states/eV per formula unit (f.u.) in the GGA calculations, which is larger than that of InNNi_3 , and its main contribution comes from Co $3d$ states which accounts for 87%. For InNNi_3 in the GGA calculations, the contribution of Ni $3d$ states to the the total DOS at the E_F (i.e., 1.803 states/eV.f.u.) accounts for 72%. These indicate the $3d$ states of transition metal atoms in

InNCu_3 and InNNi_3 play dominant roles in the total density of states of these compounds.

In order to understand the bonding nature among the ions in InNCu_3 and InNNi_3 , we analyzed the charge density contours of InNCu_3 and InNNi_3 in the (110) plane, as shown in Fig. 4. From Fig. 4, it is found that a certain amount of charges are accumulated in the intermediate region between N and Cu atoms in InNCu_3 , and slightly more charges are accumulated in the intermediate region between N and Ni atoms in InNNi_3 . This gives an evidence for the strong hybridization between N and transition metal (Cu/Ni) atoms, indicating that the N-Cu and N-Ni bondings exhibit strong covalent characteristics and the latter is slightly stronger than the former. The similar bonding characteristics for Ni-N atoms or Ni-C atoms were also found in other Ni-based ternary nitrides or carbides AXNi_3 ^{10,14,37,38}. Therefore, our results suggest that the magnetic properties of InNNi_3 reported in experiment¹⁵ are very likely due to the non-stoichiometry effect, which was also found in the cases of AlCNi_3 and GaCNi_3 ^{12,16–19}.

IV. CONCLUSIONS

In summary, we performed the first-principles calculations to study the elastic and electronic properties of cubic antiperovskites InNCu_3 and InNNi_3 . Based on the Voigt, Reuss and Hill bounds, the shear, Young's moduli and Poisson's ratio have also been estimated for the InNCu_3 and InNNi_3 polycrystals. The theoretically predicted equilibrium lattice parameters are in good agreement with the available experimental data. Our calculations show that the $3d$ states of transition metal atoms in InNCu_3 and InNNi_3 play dominant roles near the Fermi levels. InNCu_3 energetically prefers to the ferromagnetic state. The magnetic ground state of InNNi_3 , which is same to other Ni-based ternary nitrides or carbides with a cubic anti-perovskite structure, is a stable paramagnetic (non-magnetic) state. This could be understood from that the hybridization between Ni- $3d$ and N- $2p$ states in InNNi_3 is slightly stronger than the one between Cu- $3d$ and N- $2p$ states in InNCu_3 because of the more $3d$ electrons in Ni.

Acknowledgments

The author acknowledges support from National Natural Science Foundation of China under Grant No. 10674028.

- ¹ J. B. Goodenough, J. M. Longo, Magnetic and other properties of oxides and related compounds, in: K.-H. Hellwege, O. Madelung (Eds.), Landolt-Bornstein, New Series, Group III, Vol. 4a, Springer-Verlag, Berlin, 1970.
- ² M. Y. Chern, D. A. Vennos, F. J. DiSalvo, J. Solid State Chem. 96 (1992) 415.
- ³ J. Jäger, D. Stahl, P. C. Schmidt, R. Kniep, Angew. Chem. 105 (1993) 738.
- ⁴ W. S. Kim, E. O. Chi, J. C. Kim, H. S. Choi, N. H. Hur, Solid State Commun. 119 (2001) 507.
- ⁵ E. O. Chi, W. S. Kim, N. H. Hur, Solid State Commun. 120 (2001) 307.
- ⁶ T. He, Q. Huang, A. P. Ramirez, Y. Wang, K. A. Regan, N. Rogado, M. A. Hayward, M. K. Haas, J. S. Slusky, K. Inumara, H. W. Zandbergen, N. P. Ong, R. J. Cava, Nature 411 (2001) 54.
- ⁷ D. J. Singh, I. I. Mazin, Phys. Rev. B 64 (2001) 140507.
- ⁸ J. H. Shim, S. K. Keson, B. I. Min, Phys. Rev. B 64 (2001) 180510.
- ⁹ H. Rosner, R. Weht, M. D. Johannes, W. E. Pickett, E. Tosatti, Phys. Rev. Lett. 88 (2002) 027001.
- ¹⁰ S. Q. Wu, Z. F. Hou, Z. Z. Zhu, Solid State Sci. 11 (2009) 251.
- ¹¹ C. M. I. Okoye, Solid State Commun. 136 (2005) 605.
- ¹² M. Sieberer, P. Mohn, J. Redinger, Phys. Rev. Lett. 75 (2007) 024431.
- ¹³ G. H. Zhong, J. L. Wang, Z. Zeng, X. H. Zheng, H. Q. Lin, J. Appl. Phys. 101 (2007) 09G520.
- ¹⁴ S. Q. Wu, Z. F. Hou, Z. Z. Zhu, Physica B 403 (2008) 4232.
- ¹⁵ W. H. Cao, B. He, C. Z. Liao, L. H. Yang, L. M. Zeng, C. Dong, J. Solid State Chem. 182 (2009) 3353.
- ¹⁶ A. F. Dong, G. C. Che, W. W. Huang, S. L. Jia, H. Chen, Z. X. Zhao, Physica C 422 (2005) 65.
- ¹⁷ P. Tong, Y. P. Sun, X. B. Zhu, W. H. Song, Phys. Rev. B 74 (2006) 22441.
- ¹⁸ P. Tong, Y. P. Sun, X. B. Zhu, W. H. Song, Phys. Rev. B 73 (2006) 245106.

- ¹⁹ P. Tong, Y. Sun, X. Zhu, W. Song, Solid State Commun. 141 (2007) 336.
- ²⁰ S. Baroni, A. D. Corso, S. de Gironcoli, P. Giannozzi, C. Cavazzoni, G. Ballabio, S. Scandolo, G. Chiarotti, P. Focher, A. Pasquarello, K. Laasonen, A. Trave, R. Car, N. Marzari, A. Kokalj, <http://www.pwscf.org/>.
- ²¹ W. Kohn, L. J. Sham, Phys. Rev. 140 (1965) A1133.
- ²² D. M. Ceperley, B. J. Alder, Phys. Rev. Lett. 45 (1980) 566.
- ²³ J. P. Perdew, A. Zunger, Phys. Rev. B 23 (1981) 5048.
- ²⁴ J. P. Perdew, K. Burke, M. Ernzerhof, Phys. Rev. Lett. 77 (1996) 3865.
- ²⁵ A. M. Rappe, K. M. Rabe, E. Kaxiras, J. D. Joannopoulos, Phys. Rev. B 41 (1990) 1227.
- ²⁶ H. J. Monkhorst, J. D. Pack, Phys. Rev. B 13 (1976) 5188.
- ²⁷ F. Birch, Phys. Rev. 71 (1947) 809.
- ²⁸ G. Lehmann, M. Taut, Phys. Stat. Sol. (b) 54 (1972) 469.
- ²⁹ D. Sanchez-Portal, E. Artacho, J. M. Soler, Solid State Commun. 95 (1995) 685.
- ³⁰ M. J. Mehl, Phys. Rev. B 47 (1993) 2493.
- ³¹ S. Q. Wu, Z. F. Hou, Z. Zhu, Solid State Commun. 143 (2007) 425.
- ³² Z. F. Hou, Solid State Sci. 10 (2008) 1651.
- ³³ D. W. Voigt, Lehrbuch der Kristallphysik, Taubner, Leipzig, 1928.
- ³⁴ A. Reuss, Z. Angew. Math. Mech 9 (1929) 55.
- ³⁵ R. Hill, Proc. Phys. Soc. London A 65 (1952) 349.
- ³⁶ M. Mattesini, M. Magnuson, F. Tasnádi, C. Höglund, I. A. Abrikosov, L. Hultman, Phys. Rev. B 79 (2009) 125122.
- ³⁷ C. Li, W. G. Chen, F. Wang, S. F. Li, Q. Sun, S. Wang, Y. Jia, J. Appl. Phys. 105 (2009) 123921.
- ³⁸ I. R. Shein, V. V. Bannikov, A. L. Ivanovskii, Phys. Stat. Sol. (b) 247 (2010) 72.
- ³⁹ M. L. Cohen, Phys. Rev. B 32 (1985) 7988.
- ⁴⁰ S. F. Pugh, Philos. Mag. 45 (1954) 823.
- ⁴¹ D. C. Wallace, Thermodynamics of Crystals, Wiley, New York, 1972.

TABLE I: Calculated lattice constants (a , in Å), bulk modulus (B , in GPa), and the first pressure derivative B' of bulk modulus for InNC_3 and InNNi_3 . $\Delta E_{\text{tot}}^{\text{FM-PM}}$ (in eV per formula unit) is the difference between the total energies of ferromagnetic (FM) and paramagnetic (PM) states for InNC_3 and InNNi_3 . The available experimental values are also listed.

	InNC_3					InNNi_3		
	LDA		GGA		Expt. ¹⁵	LDA	GGA	Expt. ¹⁵
	PM	FM	PM	FM		PM/FM	PM/FM	
a	3.744	3.753	3.835	3.855	3.8541	3.784	3.882	3.8445
B	255.78	243.06	211.29	194.17		226.91	179.93	
B'	4.497	4.483	5.570	5.568		4.761	4.281	
$\Delta E_{\text{tot}}^{\text{FM-PM}}$	-	-0.0397	-	-0.226		0.0	0.0	

TABLE II: Calculated elastic constants (c_{11} , c_{12} , and c_{44} , in GPa), shear modulus (G , in GPa), Young's modulus (E , in GPa), and Poisson's ratio (ν) of InNCo_3 and InNNi_3 . The Voigt shear modulus (G_V , in GPa) and the Reuss shear modulus (G_R , in GPa) are also presented. For comparison, the elastic properties of InNSc_3 , ZnNNi_3 , and InCNi_3 compounds with a cubic anti-perovskite structure are listed.

Compound	Method	c_{11}	c_{12}	c_{44}	G_V	G_R	B	G	E	ν	B/G
InNCo_3	LDA	389.11	171.12	102.55	105.13	105.03	243.78	105.08	275.63	0.311	2.320
	GGA	317.54	126.76	94.98	95.14	95.14	190.35	95.14	224.67	0.286	2.001
InNNi_3	LDA	356.77	164.23	69.06	80.35	78.12	228.41	79.24	212.94	0.344	2.895
	GGA	274.08	131.20	60.01	64.58	64.11	178.83	64.35	172.37	0.339	2.779
InNSc_3	GGA ³⁶	238.57	54.28	90.76	91.31	91.31	115.71	91.31	216.88	0.188	1.267
ZnNNi_3	GGA ³⁷	354.28	134.01	48.06	72.89	62.05	207.43	67.47	182.61	0.353	3.074
	GGA ³⁸	364.20	124.90	32.69	67.47	46.09	204.67	56.78	155.92	0.373	3.604
InCNi_3	LDA ¹⁴	414.67	135.72	68.02	96.60	85.56	228.71	91.08	241.22	0.324	2.511
	GGA ¹⁴	344.20	106.30	62.68	85.19	77.31	185.60	81.25	212.70	0.309	2.284

TABLE III: Total and partial density of states at the Fermi level ($N(E_F)$, in states/eV.f.u.) for InNCo₃ and InNNi₃.

		Total density	Partial density of states		
		of states	In	N	Co ₃ /Ni ₃
InNCo ₃	LDA	3.811	0.073	0.337	3.401
	GGA	2.761	0.144	0.169	2.448
InNNi ₃	LDA	1.580	0.160	0.212	1.208
	GGA	1.803	0.180	0.256	1.367

Figure Captions

- FIG. 1: Total energy (in eV per formula unit) versus the atomic volume (in \AA^3) for InNCo_3 (upper panel) InNNi_3 (lower panel).
- FIG. 2: (Color online) Electronic band structures obtained with GGA for the majority (red solid line) and minority (blue dashed line) spins of (a) InNCo_3 and (b) InNNi_3 .
- FIG. 3: Total and partial density of states (DOS) of InNCo_3 (left panel) and InNNi_3 (right panel) obtained with the spin-polarized GGA calculations.
- FIG. 4: Charge density contours of the (110) plane for (a) InNCo_3 and (b) InNNi_3 obtained with the spin-polarized GGA calculations.

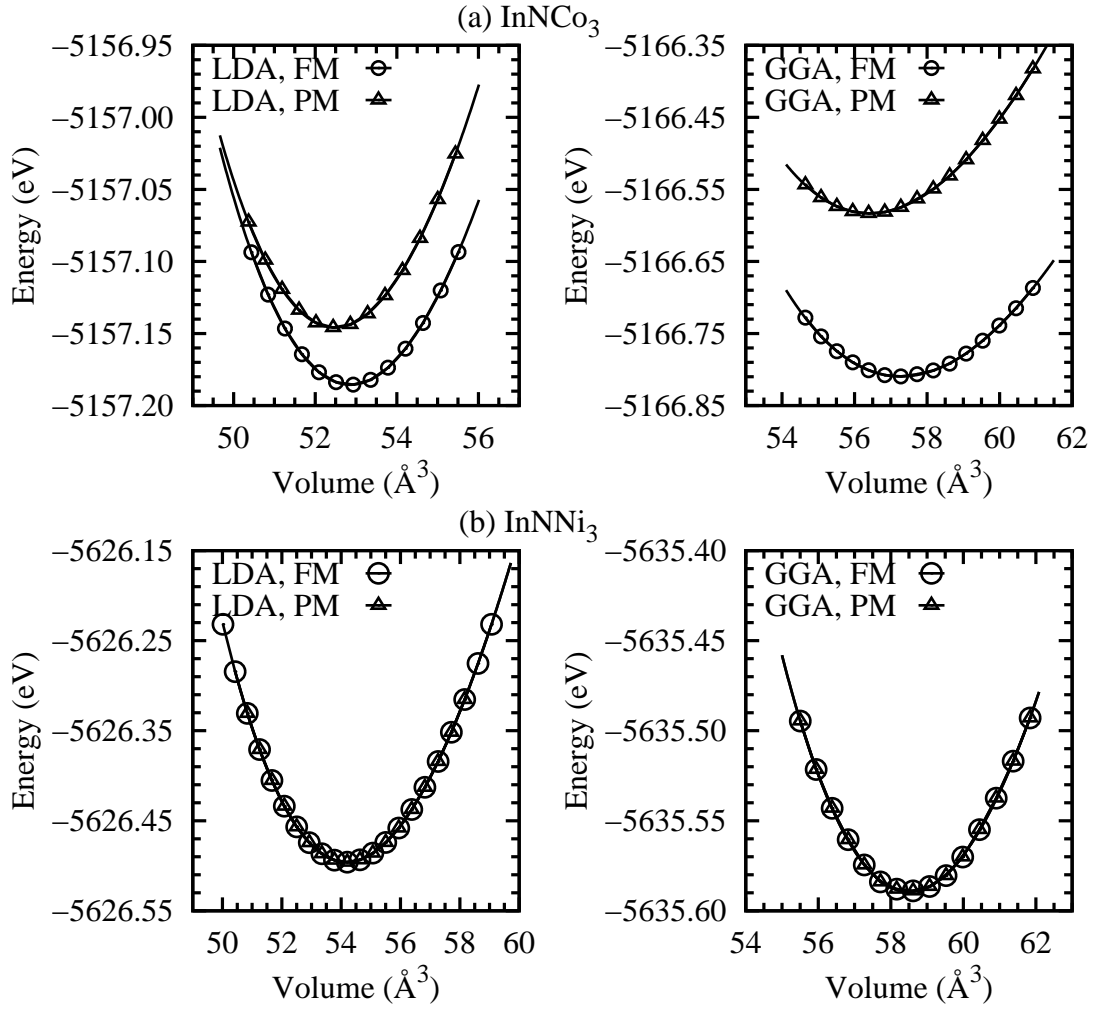


FIG. 1:

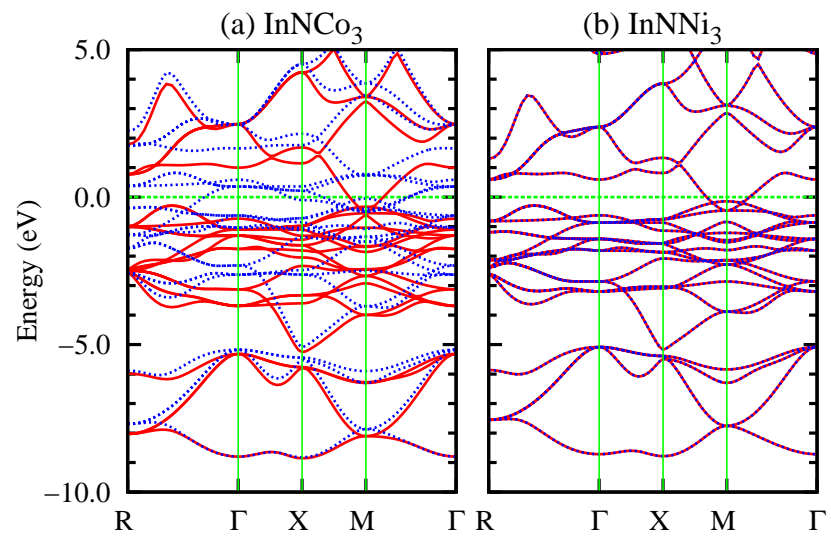


FIG. 2:

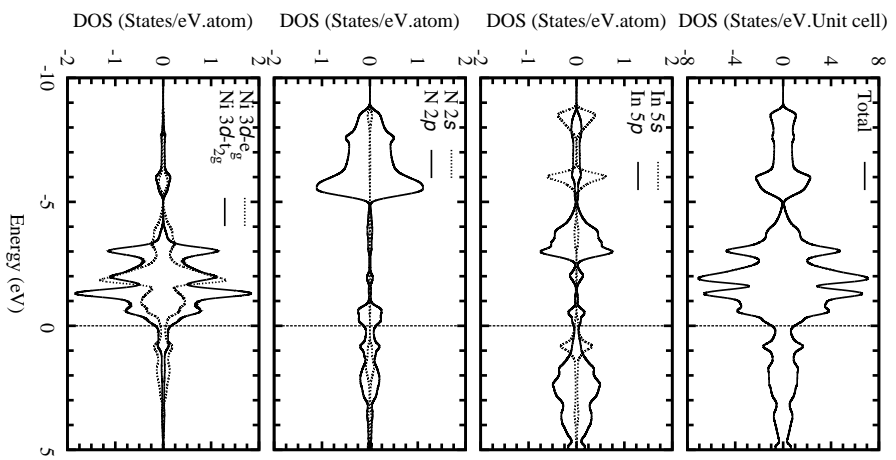
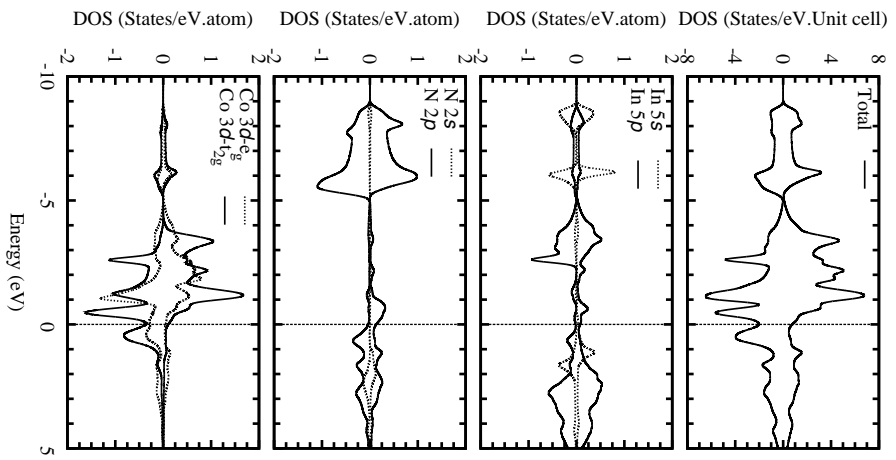


FIG. 3:

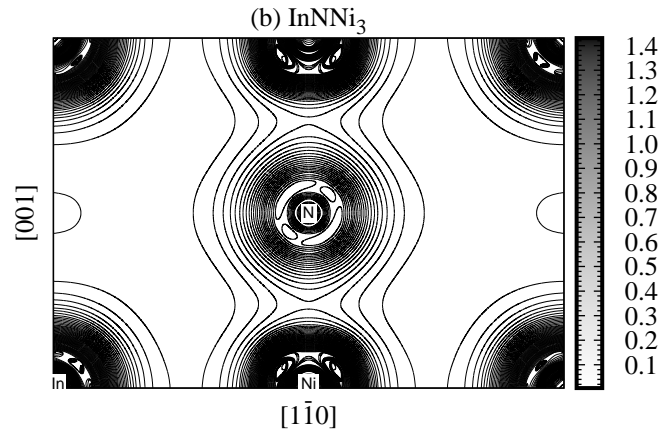
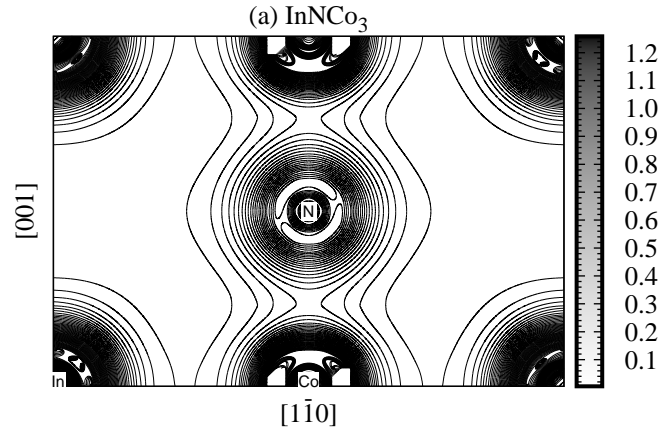


FIG. 4: